

Titan's Prolific Propane: The Cassini CIRS Perspective

C.A. Nixon^{a,b}, D.E. Jennings^b, J.-M. Flaud^c, B. Bézard^d, N.A. Teanby^e
P.G.J. Irwin^e, T.M. Ansty^f, A. Coustenis^d, S. Vinatier^d, F.M. Flasar^b

* Corresponding author: e-mail: conor.a.nixon@nasa.gov

^aUniversity of Maryland, College Park, MD 20742, USA

^bNASA Goddard Space Flight Center, Greenbelt, MD 20771, U.S.A.

^cCNRS, Universités de Paris Est and Paris 7,

61 Av. Général de Gaulle, 94010 Créteil, France

^dLESIA, Observatoire de Paris, CNRS, 5 Place Jules Janssen, 92195 Meudon Cedex, France

^eAtmospheric, Oceanic and Planetary Physics, University of Oxford, Clarendon Laboratory,

Parks Road, Oxford, OX1 3PU, UK

^fCornell University, Ithaca, NY 14853, U.S.A.

Submitted to *Planetary and Space Science*, 16 August 2018

(figures=7 tables=3)

1 Running Head:

2

Titan's Prolific Propane

3 Direct correspondence to:

4 Conor A. Nixon

5 Solar System Exploration Division

6 Planetary Systems Laboratory - Code 693

7 NASA Goddard Space Flight Center

8 Greenbelt

9 MD 20771

10 U.S.A.

11 tel. (301) 286-6757

12 fax. (301) 286-0212

13

ABSTRACT

14 Although propane gas (C_3H_8) was first detected in the stratosphere of Titan by the
15 Voyager IRIS infrared spectrometer in 1980, obtaining an accurate measurement of its
16 abundance has proved difficult. All existing measurements have been made by modeling
17 the ν_{26} band at 748 cm^{-1} : however different analyzes over time have yielded quite different
18 results, and it also suffers from confusion with the strong nearby ν_5 band of acetylene.
19 In this paper we select large spectral averages of data from the Cassini Composite In-
20 frared Spectrometer (CIRS) obtained in limb-viewing mode at low latitudes (30°S – 30°N),
21 greatly increasing the path length and hence signal-to-noise ratio for optically thin trace
22 species such as propane. By modeling and subtracting the emissions of other gas species,
23 we demonstrate that at least six infrared bands of propane are detected by CIRS, in-
24 cluding two not previously identified in Titan spectra. Using a new line list for the range
25 1300 – 1400 cm^{-1} , along with an existing GEISA list, we retrieve propane abundances from
26 two bands at 748 and 1376 cm^{-1} . At 748 cm^{-1} we retrieve $4.2 \pm 0.5 \times 10^{-7}$ ($1\text{-}\sigma$ error) at 2
27 mbar, in good agreement with previous studies, although lack of hotbands in the present
28 spectral atlas remains a problem. We also determine $5.7 \pm 0.8 \times 10^{-7}$ at 2 mbar from the
29 1376 cm^{-1} band - a value that is probably affected by systematic errors including contin-
30 uum gradients due to haze and also an imperfect model of the ν_6 band of ethane. This
31 study clearly shows for the first time the ubiquity of propane's emission bands across the
32 thermal infrared spectrum of Titan, and points to an urgent need for further laboratory
33 spectroscopy work, both to provide the line positions and intensities needed to model
34 these bands, and also to further characterize haze spectral opacity. The present lack of
35 accurate modeling capability for propane is an impediment not only for the measurement
36 of propane itself, but also for the search for the emissions of new molecules in many spec-
37 tral regions.

**key words=TITAN ATMOSPHERE; ATMOSPHERIC ABUNDANCES,
OUTER PLANETS; PROPANE; INFRARED SPECTROSCOPY;
ABUNDANCE RETRIEVAL**

39 1 Introduction

40 Propane (C_3H_8) was first detected in the atmosphere of Titan by the Voyager 1 IRIS
41 spectrometer during the 1980 encounter (Maguire et al., 1981), when excess emission at
42 748, 922, 1053 and 1158 cm^{-1} was used to make the identification. Propane is an end-
43 product of Titan’s active photochemistry. This process begins when methane is dissociated
44 in the upper atmosphere by UV photons and energetic particles to form hydrocarbon
45 radicals and ions, which undergo a complex chain of reactions to form larger molecules
46 and haze particles. The main pathway leading to C_3H_8 is the three-body association: CH_3
47 $+ \text{C}_2\text{H}_5 + \text{M} \rightarrow \text{C}_3\text{H}_8 + \text{M}$ (Yung et al., 1984; Wilson and Atreya, 2004), and most is
48 ultimately removed by condensation in the lower stratosphere. Spectrally, propane is a
49 very important molecule, as it has 27 predicted infrared vibrational modes of which at
50 least 23 are active (see §4.1).

51 Early attempts to measure the abundance of propane from the Voyager dataset suffered
52 from a lack of reliable laboratory spectroscopic data, resulting in initial over-estimates
53 followed by a downward trend of revised abundances until the mid-1990s. Maguire et al.
54 (1981) used laboratory spectra to compute the band intensity of the 748 cm^{-1} band,
55 thereby inferring a uniformly-mixed abundance for Titan’s stratosphere of 2×10^{-5} , with
56 an uncertainty factor of three. The value was halved the next year by Kim and Caldwell
57 (1982), who modeled the same band to obtain a propane abundance of 1.2×10^{-5} .
58 Coustenis et al. (1989a) also used a band-model approach, based on newly measured ab-
59 sorptions from Giver et al. (1984), and a full radiative transfer treatment to greatly revise
60 the estimate for uniformly-mixed stratospheric propane downwards to $(7 \pm 4) \times 10^{-7}$ at
61 the equator.

62 In 1991 ~ 9000 lines representing the 748 cm^{-1} band were added to the GEISA atlas
63 (Husson et al., 1992), with the data taken from unpublished measurements at NASA

64 GSFC by G. Bjoraker circa 1986. These allowed Coustenis and Bézard (1995) to make a
65 full line-by-line model of the blended C_2H_2 and C_3H_8 emissions. For the first time, the
66 latitude variation of propane was reported: a modest increase from $5.0 \pm 1.7 \times 10^{-7}$ at
67 the equator to $1.2 \pm 0.5 \times 10^{-6}$ at 70°N (assuming uniform stratospheric abundances).
68 Simultaneously, enhancements in many other minor gases were detected in the northern
69 (winter) polar stratosphere: especially in the heavier, acetylene-derived gases (C_4H_2 , C_3H_4 ,
70 HC_3N , C_2N_2), but also HCN and C_2H_4 . These enhancements have been modeled and
71 explained dynamically, as due to downward advection of short-lived species at the pole(s)
72 in a global circulation cell(s), as these molecules tend to have higher abundances at higher
73 altitudes in the absence of dynamics (Teanby et al., 2009; Lebonnois et al., 2009, and
74 references therein).

75 The launch of the Infrared Space Observatory (ISO) in 1995 provided a new tool
76 for studying planetary atmospheres. In 1997, the Short Wavelength Spectrometer (SWS)
77 was used to acquire spectra of Titan with a mean resolution of 0.4 cm^{-1} - an order of
78 magnitude improvement over the 4.3 cm^{-1} of Voyager IRIS, although spatially unresolved.
79 Low-latitude gaseous abundances were reported by Coustenis et al. (2003), and included
80 a measurement of $q_{\text{C}_3\text{H}_8} = 2 \pm 1 \times 10^{-7}$ via the same (748 cm^{-1}) band as Voyager IRIS.
81 The reason for this slightly lower value is unclear, although real seasonal change might
82 be a factor, as well as the higher spectral resolution.

83 Even this improved spectral resolution was insufficient to actually separate the emis-
84 sion lines of propane at 748 cm^{-1} from those of the R-branch lines of the 729 cm^{-1} (ν_5)
85 band of C_2H_2 , and weaker contributions from HCN and C_2H_6 . The first study to resolve
86 the C_3H_8 emission features from the other gases was made by Roe et al. (2003), who used
87 the $R \simeq 10^5$ TEXES Echelle Spectrograph attached to the NASA Infrared Telescope Facil-
88 ity (IRTF) to make high spectral resolution, disk averaged observations of Titan, resulting
89 in a stratospheric abundance estimate of $(6.2 \pm 1.2) \times 10^{-7}$ at 90–250 km (13.0–0.24 mbar),

90 in agreement with the low-latitude IRIS values. It is important to note that these authors
91 compared four line lists for the 748 cm^{-1} propane band then available, noting significant
92 discrepancies between all the lists and actual propane spectral data. Only the absorption
93 coefficients that they derived empirically from laboratory data provided a good fit to the
94 planetary data. In addition, this was the first study of Titan’s propane to use the ν_{26}
95 designation for this band, rather than the ν_{21} designation that was commonly used by
96 earlier authors. We discuss the dichotomy of propane band designations further in section
97 4.1.

98 In 2004 the Cassini/Huygens spacecraft entered orbit around Saturn, opening a new
99 era in Titan research. The Composite Infrared Spectrometer (CIRS) instrument onboard
100 Cassini is a successor to the Voyager IRIS, although with many improvements including
101 to spectral range and resolution, and spatial resolution (see Section 2.1). Furthermore,
102 the great variety of Titan flyby encounter ranges and relative orbital inclinations, com-
103 bined with the much greater available observing time versus the Voyager encounters,
104 permits Cassini CIRS to make a very diverse range of scientific investigations. These in-
105 clude low-spectral resolution North–South surface temperature mapping (Jennings et al.,
106 2009) and limb temperature mapping (Achterberg et al., 2008), through to high spectral
107 resolution composition measurements on both the disk and the limb (Coustenis et al.,
108 2007; Vinatier et al., 2007a; Teanby et al., 2008b, and references therein), with vertical
109 resolution of better than one scale height (40–50 km).

110 So far, two analyses of CIRS Titan spectra have considered propane. Coustenis et al.
111 (2007) modeled zonally-averaged sets of mid-infrared spectra ($600\text{--}1400\text{ cm}^{-1}$) from 70°S –
112 70°N to measure the latitude variations in hydrocarbons, nitriles and CO_2 , including the
113 748 cm^{-1} band of propane for which spectral line data is available in GEISA. C_3H_8 was
114 found to exhibit a very slight increase from the south to the north, from $\sim 5 \times 10^{-7}$
115 to $\sim 8 \times 10^{-7}$. Vinatier et al. (2007a) modeled two high spectral resolution (0.5 cm^{-1})

116 observation sets of Titan’s limb, from the Tb and T3 flybys and directed at 15°S and
117 80°N respectively. C₃H₈ was found to display an increasing abundance with altitude in
118 the range ~150–350 km (~ 2.0–0.01 mbar) at both latitudes, in accordance with the
119 conventional understanding of photochemical formation in the upper atmosphere and
120 downward advection to the lower stratosphere where removal through condensation occurs
121 (89% according to Wilson and Atreya, 2004).

122 In this paper we have two objectives. First, we show clearly the very prolific extent
123 of the multiple propane bands that can be detected by CIRS across the mid-infrared.
124 At least six bands are visible in limb spectra after the modeling and removal of other
125 stronger gas emissions. Second, we use a new laboratory line list for propane in the
126 range 1300–1400 cm⁻¹ (Flaud et al., 2001), along with the GEISA list for the 748 cm⁻¹
127 band to make independent measurements of the propane abundance, and show that the
128 results are probably compatible when systematic errors are accounted for. Finally, we
129 draw conclusions about the current status of propane retrievals in the thermal infrared.

130 **2 Data Acquisition**

131 In this paper we make use of two spectral datasets. The first is a set of Titan limb
132 spectral data, acquired by Cassini CIRS between 2004 and 2008. The second is a set
133 of laboratory absorption spectra of room temperature propane gas acquired at Pacific
134 Northwest National Laboratory in 2002. Both datasets are now described.

135 *2.1 Cassini CIRS Limb Observations*

136 The Composite Infrared Spectrometer (CIRS) carried on-board Cassini is a dual
137 Fourier Transform interferometer design (Kunde et al., 1996; Flasar et al., 2004). A shared

138 telescope and foreoptics feed incoming radiation simultaneously into two interferometers:
139 a Martin-Puplett (polarizing) type optimized for far-infrared rays ($10\text{--}600\text{ cm}^{-1}$), and
140 a conventional Michelson design for the mid-infrared ($600\text{--}1400\text{ cm}^{-1}$). The recombined
141 beam of the far-infrared interferometer is focused onto a single circular bolometer detec-
142 tor, known as focal plane 1 (FP1), while mid-infrared detection capability is provided by
143 two 1×10 HgCdTe arrays: focal plane 3 (FP3, $600\text{--}1100\text{ cm}^{-1}$) and focal plane 4 (FP4,
144 nominal range $1100\text{--}1400\text{ cm}^{-1}$, see also Appendix A). Both interferometers also share a
145 common scan mirror mechanism and reference laser. The spectral resolution is determined
146 by the commanded scan time, and is variable from 15.5 to 0.5 cm^{-1} .

147 At 5–9 hours from closest approach to Titan ($1.0\text{--}1.8 \times 10^5$ km range), the CIRS in-
148 strument makes observations of the atmospheric limb, placing the mid-infrared arrays
149 perpendicular to the disk edge, and obtaining spectral samples at $\sim 30\text{--}50$ km resolution,
150 equivalent to approximately one atmospheric scale height. These observations come in two
151 types: (i) temperature maps (shorter dwell, 15.5 cm^{-1} spectral resolution, repositioning
152 at multiple latitudes) and (ii) composition integrations (longer dwell, 0.5 cm^{-1} resolution,
153 single latitude).

154 For the purpose of identifying the weak emission bands, we have created large averages
155 of low-latitude spectra for FP3 and FP4 from the high spectral resolution limb integrations
156 (type (ii) above). Note that we do not attempt to explore the vertical and latitudinal
157 variation of the propane abundance from the CIRS dataset, which has been documented
158 elsewhere (Coustenis et al., 2007; Vinatier et al., 2007a, 2009), but rather to maximise
159 signal-to-noise to emphasize and detect very weak emission features while still maintaining
160 reasonable homogeneity of the dataset.

161 Therefore we chose to average across all flybys from the prime mission (June 2004 to
162 June 2008) and latitudes in the range $30^\circ\text{S}\text{--}30^\circ\text{N}$, in the knowledge that Titan’s strato-

163 sphere is slowly varying in this temporal and spatial interval (Coustenis et al., 2007;
 164 Achterberg et al., 2008; Teanby et al., 2008a). However, Titan’s atmosphere varies much
 165 more rapidly in the vertical direction, and therefore we restricted our averages to 100–
 166 150 km (pixel centers) where the signal-to-noise ratio was found to be the most favorable.
 167 The spacecraft distance range was also constrained to be less than 2×10^5 km. See Table
 168 I for additional details.

169 **[TABLE I]**

170 2.2 PNNL Laboratory Spectroscopy

171 For comparison with the CIRS spectra, Dr Steven Sharpe at Pacific Northwest National
 172 Laboratories (PNNL), has shared with us room temperature (296 K) absorption spectra
 173 of propane gas, taken as part of a large-scale survey of molecular infrared spectra. These
 174 consist of 6 individual co-added spectra of 98% pure propane gas measured with a Bruker-
 175 66V FTIR at 0.112 cm^{-1} unapodized resolution, covering the FP3 and FP4 part of the
 176 CIRS spectral range (600–1400 cm^{-1}). Full experimental details have been published in
 177 the literature (Sharpe et al., 2004).

178 We have convolved the PNNL spectra with a Hamming kernel $h(\Delta\tilde{\nu})$ (instrumental
 179 line shape) of FWHM 0.48 cm^{-1} for approximate comparison with the CIRS spectra,
 180 which originate at much lower temperatures ($\sim 160 \text{ K}$) in Titan’s stratosphere:

$$181 \quad h(\Delta\tilde{\nu}) = \frac{a \left(1.08 - 0.64a^2 [\Delta\tilde{\nu}]^2\right) \text{sinc}(2\pi a\Delta\tilde{\nu})}{1 - 4a^2 [\Delta\tilde{\nu}]^2} \quad (1)$$

182 where h is the weighting factor at each position $\Delta\tilde{\nu} = (\tilde{\nu} - \tilde{\nu}_0)$ relative to a given
 183 wavenumber $\tilde{\nu}_0$ in the original spectrum, and a is an effective path difference: $a =$
 184 $1.815/(2 \times 0.48) = 1.89 \text{ cm}$ that compensates the Nyquist path difference at the de-

185 sired resolution ($1/(2 \times 0.48)$ cm) for the FWHM of the Hamming function in Nyquist
186 units (1.815). Note that h is normalized so that: $\int h(\Delta\tilde{\nu}) d(\Delta\tilde{\nu}) = 1.0$ over the desired
187 interval: we used ± 10 samples relative to each wavenumber (21-pt kernel).

188 3 Data Analysis

189 3.1 Model Atmosphere

190 Our model atmosphere consists of 100 layers equally spaced in $\log(p)$ from the sur-
191 face (1.45 bar) to 700 km (4×10^{-8} bar.) The initial temperature-pressure profile is a
192 smoothed version of the Huygens HASI results (Fulchignoni et al., 2005) (covering from
193 the surface to 7×10^{-12} bar at 10°S , 168°E) with heights calculated from hydrostatic
194 equilibrium. All gases known to be relevant for the 700–1400 cm^{-1} range of Titan’s in-
195 frared spectrum are included, namely: N_2 , CH_4 , H_2 , HCN , C_2H_2 , C_2H_6 , C_2H_4 and C_3H_8 .
196 In addition, the isotopologues $^{13}\text{C}^{12}\text{CH}_2$, $^{13}\text{CH}_4$, CH_3D and $^{13}\text{CH}_3\text{D}$ are included as sepa-
197 rate species. The initial abundances and isotopic ratios mostly follow the Huygens GCMS
198 results (Niemann et al., 2005) and previous measurements by CIRS pertaining to low lat-
199 itudes (Coustenis et al., 2007). In particular, H_2 and C_2H_4 are uniformly mixed, while
200 CH_4 follows the GCMS profile, N_2 is defined as $q_{\text{N}_2} = 1.0 - q_{\text{CH}_4}$, and the other gas
201 primary isotopologues, with the exception of C_2H_2 , have constant abundances in the
202 middle atmosphere, and follow condensation profiles towards the tropopause. The C_2H_2
203 VMR, which is known to have a gradient at low-latitudes, follows the 10°S profile of
204 Vinatier et al. (2007a). Finally, the minor isotopologue species have initial profiles scaled
205 from the primary isotopologue by molecular isotopic ratios previously determined by CIRS
206 (Bézard et al., 2007; Nixon et al., 2008a). Fig. 1 shows the initial gas profiles.

Fig. 1. Appears Here.

207 Finally, our model atmosphere also includes a single aerosol component with constant
208 mass mixing ratio of particles above the tropopause (45 km) as described in Nixon (1998).

209 3.2 Forward Spectral Model

210 The forward model (NEMESIS, Irwin et al., 2008) computes the emerging radiation
211 field for Titan limb rays using the correlated- k approximation (Lacis and Oinas, 1991) for
212 rapid calculation of atmospheric opacity. The three types of opacity included are: gas vi-
213 brational bands, collision-induced absorption (CIA) of N_2 , CH_4 and H_2 , and aerosol/haze
214 opacity. The k -coefficients for gaseous bands and CIA opacities are computed and pretab-
215 ulated over the full range of pressures and temperatures required for the Titan model
216 atmosphere, as well as the CIRS full spectral range, to enable rapid calculations. The
217 spectral opacities are pre-convolved with a Hamming apodization function of FWHM
218 0.48 cm^{-1} , and 50 g -ordinates are used to approximate the k -distributions in each spec-
219 tral bin.

220 Spectral line data are taken from the HITRAN 2004 (for CH_4 ν_4 1304 cm^{-1} , HCN ν_2
221 712 cm^{-1} and C_2H_4 ν_7 949 cm^{-1} ; Rothman et al., 2005) and GEISA 2003 (for C_2H_2 ν_5 729
222 cm^{-1} , C_3H_8 ν_{26} band; Jacquinet-Husson et al., 2005) atlases. We also used supplemental
223 sources of line data for the C_2H_6 ν_9 band (822 cm^{-1} Vander Auwera et al., 2007), for
224 $^{13}\text{CH}_3\text{D}$ (ν_6 1156 cm^{-1} Bézard et al., 2007) and for the $1300\text{--}1400 \text{ cm}^{-1}$ bands of C_3H_8
225 (mostly due to the ν_{18} 1376 cm^{-1} and the ν_{19} 1338 cm^{-1} Flaud et al., 2001) that post-
226 date the most recently available GEISA and HITRAN atlases. We made additional scaling
227 corrections to the line strengths for the ν_{26} band of C_3H_8 , and also to the line width and
228 temperature dependence parameters for both the GEISA and the Flaud et al. (2001) line
229 lists, justified in detail in Appendix B.

230 Additionally, for the ν_6 (1378 cm^{-1}) and ν_8 (1468 cm^{-1}) bands of C_2H_6 , which are not

231 included in any current line atlases, we used a ‘pseudo-linelist’ made publicly available by
232 the Jet Propulsion Laboratory ([http:// mark4sun.jpl.nasa.gov/pseudo.html](http://mark4sun.jpl.nasa.gov/pseudo.html)). This list is
233 an approximation which seeks to model the overall absorption of these bands by using a
234 uniform distribution of ‘pseudo’ lines of varying strengths, without actual knowledge of
235 the real line positions or intensities.

236 To fit the continuum we used two further sources of opacity; (i) collision-induced
237 opacity of six molecular pairs of H₂, N₂ and CH₄ (see detailed references in Teanby et al.,
238 2006), and (ii) a simple haze with a constant (scaleable) number of particles per gram
239 of atmosphere above the tropopause. The haze had either (A) a uniform grey spectral
240 absorption, or (B) a spectral absorption cross-section derived by applying Mie theory to
241 0.2 μm radius spheres (no scattering), using the real and imaginary refractive index data
242 for laboratory haze analogue (tholin) as measured by Khare et al. (1984).

243 Previously, most models of CIRS Titan mid-infrared limb spectra (Teanby et al., 2007;
244 Vinatier et al., 2007a,b; Nixon et al., 2008b; Jennings et al., 2008; Coustenis et al., 2008)
245 have used the approximation of a single limb ray originating from the center of the detec-
246 tor fields of view (FOVs) projected onto the limb: the ‘infinitesimal’ FOV approximation.
247 However, Teanby and Irwin (2007) have investigated the spatial smoothing effect of the
248 small but finite mid-IR detector FOVs when applied to Titan limb sounding. They con-
249 clude that approximating a limb view using an infinitesimal ray introduces non-negligible
250 errors when the highest spectral resolution of CIRS (0.5 cm⁻¹) is used and many spectra
251 are co-added to lower the NESR.

252 More recently Nixon et al. (2009) have analyzed laboratory and in-flight field-of-view
253 response measurements of CIRS, and computed real 1-D spatial response functions for
254 all 20 mid-infrared detectors. Using these functions, they investigated systematic errors
255 introduced by either the infinitesimal ray approximation or the finite (or ‘boxcar’) ap-

256 proximation for Titan limb viewing, relative to using the real detector spatial responses.
 257 Their conclusion was that, for limb averages of as few as 20 spectra, the errors due to
 258 both approximations became significant compared to the noise level.

259 Therefore, in this work we have included the actual 1-D spatial responses for each
 260 detector as follows. For the n^{th} individual spectrum, recorded by detector m , let a_n be
 261 the tangent altitude (in km) at the FOV center projected onto Titan’s limb and d_n be the
 262 spacecraft-tangent point distance in km. Then the n^{th} spatial weighting function quantized
 263 onto a vertical grid z_i of 1-km altitude increments is then (c.f. Eq. 10 of Nixon et al., 2009):

$$w_n(z_i) = \frac{\bar{R}_m((z_i - a_n)/d_n)}{\sum_i \bar{R}_m((z_i - a_n)/d_n)} \quad (2)$$

264 .

265 Where \bar{R}_m is the 1-D (Y -averaged) response function of detector m expressed in angular
 266 units (tabulated in Table 4 of Nixon et al., 2009). For the average of all N spectra then
 267 the spatial weighting function is:

$$W(z_i) = \frac{1}{N} \sum_{n=1}^N w_n(z_i) \quad (3)$$

269 .

270 This ‘effective’ spatial weighting function is used to compute a mean model spectrum, by
 271 weighting synthetic spectra calculated for limb rays at each altitude:

$$\bar{I}(\tilde{\nu}) = \sum_{z=z_{\min}}^{z=z_{\max}} W(z_i) I(z_i, \tilde{\nu}) \quad (4)$$

273 where z_{\min} and z_{\max} are the lowest and highest altitudes where $W(z_i) \neq 0$, and $\tilde{\nu}$ is
 274 wavenumber.

275 In practice, the 1 km resolution calculation grid is both unnecessarily fine to achieve

276 sufficient modelling accuracy, and also prohibitively slow, as it necessitates the calculation
277 of ~ 50 individual limb rays to produce a single spectrum at each modelling iteration. We
278 performed trial retrievals at various grid spacings, finding that 5 km grid point spacing
279 is sufficient for $> 99\%$ accuracy on both FP3 and FP4 (at which level the accuracy
280 becomes dominated by other effects, such as knowledge of limb pointing), and we therefore
281 interpolated the function $W(z_i)$ at 5 km increments relative to the mean limb tangent
282 altitude of the average spectrum, cutting off at a minimum weighting of 0.001. 5 km
283 resolution is approximately 10% of the scale height in Titan’s lower stratosphere.

284 The resampled $W(z_i)$ functions in 5 km steps for the FP3 and FP4 spectral averages
285 analyzed herein are shown in Fig. 2.

Fig. 2. Appears Here.

286 3.3 Retrieval Algorithm

287 The retrieval algorithm is a mathematical formalism used to find the ‘optimal estimate’
288 set of model parameters, by iteration (Rodgers, 2000). At each step of the retrieval, the
289 forward model is used to calculate a synthetic spectrum, as described above, which is
290 then compared to the data spectrum. A cost function is calculated which is similar to
291 a χ^2 test of the difference between the data and model spectrum, with an additional
292 term to provide smoothing of the solution, also known as the a priori constraint. Model
293 parameters are then adjusted along the downhill gradients that tend to decrease the cost
294 function, so that divergence between the model and data will be reduced on the next step.
295 When a preset convergence limit is reached - i.e. when the percentage change in the cost
296 function falls below a threshold value, the retrieval ceases. This algorithm is identical to
297 that used in Nixon et al. (2008a) - see also Irwin et al. (2008) for further details.

298 **4 Results**

Fig. 3. Appears Here.

299 In this study we first used the $1225\text{--}1325\text{ cm}^{-1}$ spectral region of the ν_4 methane band
300 to retrieve atmospheric temperatures, holding the methane abundance constant. Fig. 3
301 shows the result. Note that the retrieved temperatures in the main information region
302 of the lower stratosphere are significantly colder than the HASI profile, by as much as
303 10 K - much greater than expected due to latitude variation alone (HASI = 10°S ; CIRS
304 = 2°N). This discrepancy has been noted and remarked on in several previous studies of
305 CIRS data (see §2 of Flasar and Achterberg, 2009, and references therein), and can be
306 seen to be part of a larger difference where the HASI stratopause is considerably lower
307 (by $\sim 60\text{km}$) than that determined by fitting CIRS data. The spectroscopic parameters
308 for the methane ν_4 band are well-studied, and the CIRS data cannot be reconciled with
309 the HASI temperature profile, so a solution to this problem has not yet been reached.

310 The error on the temperature profile includes both spectral noise and also the 5%
311 uncertainty on the Huygens GCMS methane abundance quoted by Niemann et al. (2005).
312 See Nixon et al. (2008a) for description of the error propagation. Fig. 4 shows the vertical
313 error variation.

Fig. 4. Appears Here.

314 The temperature profile was then fixed, and we carried out numerous separate re-
315 trievals on specific spectral regions suspected to harbor propane emission bands. In these
316 retrievals, the grey ‘aerosol’ opacity was scaled to obtain a fit to the continuum level, and
317 simultaneously relevant minor gas VMR profiles for each spectral region were adjusted to
318 fit the emission bands.

319 Two separate models were calculated for each spectral region: (i) a best fit spectrum
320 without propane, to reveal the propane signature in the residual, and (ii) for spectral

321 regions where C_3H_8 line data were available, we fitted a model for all gases including
322 propane, to obtain a C_3H_8 abundance, allowing the values from multiple C_3H_8 bands to
323 be intercompared. The results are now discussed in detail.

324 4.1 Propane Band Detections

325 Figs. 5 and 6 show the results of modeling various CIRS spectral regions that were
326 candidates for propane emissions. In each figure, the left hand column shows the data
327 spectrum and model (grey haze used), while the right hand column shows the residual
328 after subtraction of model from data, along with the corresponding portion of the PNNL
329 laboratory absorption spectrum. The laboratory spectrum has been convolved with a 0.48
330 cm^{-1} Hamming kernel for direct comparison to CIRS data, and arbitrary scaling is used.

Fig. 5. Appears Here.

Fig. 6. Appears Here.

331 Four strong bands are clearly detected on FP3 and four on FP4, as indicated on the
332 figures, along with the locations of several weaker undetected bands. Note that the band at
333 1053 cm^{-1} is detected on both FP3 and FP4 where the spectral ranges overlap. The band
334 assignments for all vibrational modes of C_3H_8 are listed in Table II. At this juncture, we
335 are obliged to discuss a confusion regarding propane band numbering in the pre-existing
336 literature.

337 [TABLE II]

338 Historically, there has been some inconsistency over the actual band designations for
339 propane's infrared spectrum. This appears to be traceable to two original studies - a 1965
340 paper by Gayles and King, hereafter GK65, and a 1972 paper by Shimanouchi, hereafter
341 S72 - that introduced differing numbering schemes (see Table II). The GK65 scheme was

342 apparently followed by Maguire et al. (1981), Giver et al. (1984) and all subsequent anal-
343 yses of the IRIS dataset, and thence propagated into the Cassini CIRS community. The
344 S72 scheme however was adopted by Flaud et al. (2001), Roe et al. (2003) and also by the
345 U.S. National Institute of Standards and Technology (NIST), and appears preferable now
346 both because of that official endorsement, and also because all 27 predicted vibrational
347 modes are accounted for. Therefore, we use the S72/NIST numbering scheme in this work.
348 Table II lists both sets of band designations as an aid to translating band numbers from
349 earlier works (especially Voyager papers).

350 Under the NIST numbering scheme, we clearly detect the ν_{26} (748 cm^{-1}), ν_{21} (922
351 cm^{-1}) and ν_{20} (1053 cm^{-1}) bands on FP3, which all have strong central Q-branch peaks.
352 All three of these bands were claimed to be detected by Voyager (Maguire et al., 1981).
353 Note that the shape of the ν_{21} band appears somewhat different at room temperature
354 (PNNL spectrum) compared to the colder Titan spectrum, due to the presence of hot
355 bands on the short-wavelength side of the fundamental in the lab spectrum. The ν_8 band
356 on the other hand lacks a Q-branch, and the detection is uncertain at this time, although
357 we do appear to see a minimum in the right location near the band center at 869 cm^{-1} .
358 Note that the residual of the ethane fitting appears surprisingly large, given that we are
359 using very recently updated line parameters for the ν_9 band (Vander Auwera et al., 2007).
360 This appears to be caused by trying to minimize the overall χ^2 fit, in the presence of the
361 non-flat continuum.

362 We must be careful here to emphasize possible aerosol effects: a non-grey aerosol could
363 easily account for some or all of the gradient in the residual. So long as we cannot positively
364 distinguish between the two opacity sources, the propane ν_8 detection should be regarded
365 as still somewhat tentative. A clear way to make progress would be to derive spectroscopic
366 parameters for the band from lab data and include it in the gas model: any remaining
367 residual gradient would then likely be due to aerosol alone.

368 On FP4, the strongest propane feature inside the clean spectral range (1100–1400
369 cm^{-1}) is the Q-branch of ν_{18} at 1376 cm^{-1} . The ν_7 band (1158 cm^{-1}) is similar in shape
370 to the ν_8 of FP3, and is also evident here after the modeling/removal of CH_3D and $^{13}\text{CH}_3\text{D}$
371 emissions. In previous works, this band has sometimes been modeled with a band opacity
372 model to improve the D/H determination (e.g. Coustenis et al., 1989b). Other weaker Q-
373 branch peaks of ν_{25} (1192 cm^{-1}) and ν_{19} (1338 cm^{-1}) fall inside the FP4 nominal range,
374 but are at the noise level.

375 Proceeding with caution outside the nominal range (see Appendix A), we see a clear
376 signal of the Q-branch of ν_{20} (1053 cm^{-1}), with improved signal-to-noise (S/N) over
377 the FP3 detection. (We can discount aliasing here, as there is no noticeable emission at
378 the aliased frequency of 987 cm^{-1} .) In the short-wavelength non-clean band, we also
379 apparently detect the Q-branch peak of ν_{24} (1472 cm^{-1}), although it is apparent here that
380 significant residual remains after modeling which is not attributable to propane. There
381 may be several factors at work here to undermine our model: (i) the ethane pseudo-linelist
382 is likely to be imperfect; (ii) the ethane ν_8 (1468 cm^{-1}) and ν_{11} (1469 cm^{-1}) bands remain
383 strong out to $\sim 1600 \text{ cm}^{-1}$, and therefore will contribute significantly through aliasing
384 (‘folding’ around 1529 cm^{-1}); (iii) the continuum may have haze opacity that is difficult
385 to assess in the presence of the other uncertainties.

386 4.2 Propane Gas Abundance

387 Having demonstrated the detection of multiple propane bands by CIRS, we wished
388 to model those for which line data is available. As stated earlier, only the ν_{26} band at
389 748 cm^{-1} has been previously analyzed to obtain abundances of C_3H_8 on Titan, due to
390 its unique availability in an existing atlas (GEISA). However, due to more recent work
391 by Flaud et al. (2001), line parameters for propane bands in range $1300\text{-}1500 \text{ cm}^{-1}$ were

392 available to us, allowing the new possibility of retrieving propane abundances from these
393 bands also. After some experimentation, we concluded that accurate modeling of the
394 ν_{24} band at 1472 cm^{-1} was not possible, due to the uncertainties in ethane and haze
395 opacity, combined with the complexity of folding the (unknown) aliased spectrum above
396 1529 cm^{-1} . However, fitting the ν_{18} at 1376 cm^{-1} proved to be a more tractable problem.

397 We used two spectral windows for the abundance measurements: $740\text{--}760\text{ cm}^{-1}$ (ν_{26})
398 and $1370\text{--}1390\text{ cm}^{-1}$ (ν_{18}), choosing relatively narrow spectral regions to avoid the effects
399 of, respectively, the very strong acetylene band at 729 cm^{-1} and large instrumental noise
400 spike at 768 cm^{-1} (FP3), and a non-flat continuum that showed apparent broad haze
401 features at the scale of $\sim 20\text{ cm}^{-1}$ (FP4). Haze spectral features are the intended subject
402 of a future study, and are not pursued further herein.

403 We then added propane gas back into the model atmosphere and separately retrieved
404 its best-fit abundance for each window using the previously determined temperature pro-
405 file. Our objective was not to determine the absolute abundance of propane at a single
406 altitude to high accuracy, where we could have fitted all regions simultaneously, but rather
407 to compare the relative results for FP3 and FP4. Early retrieval attempts using these win-
408 dows alerted us to a problem with the GEISA line strengths for the ν_{26} band, which is
409 described in detail in Appendix B. This problem was remedied by rescaling the spectral
410 lines prior to the final retrievals.

Fig. 7. Appears Here.

411 The final results of the fitting are shown in Fig. 7. The red line shows the residual for
412 a forward-model calculation using the retrieved abundances of all gases except propane,
413 which is removed to show its contribution. The other lines show the residual after fitting
414 with all gases including propane and either grey haze (blue line) or tholin haze (green
415 line). The fits with the two haze models are indistinguishable over the narrow 20 cm^{-1}

416 window.

417 **[TABLE III]**

418 The individual abundances determined from each model fit are given in Table III,
419 along with errors. Included in the error calculation (added in quadrature) are (i) the 1-
420 σ random noise on the spectrum; (ii) propagated temperature retrieval error from two
421 sources, (a) the spectral noise from the temperature retrieval, and (b) the 5% uncertainty
422 in the methane abundance quoted by Niemann et al. (2005), combined as described in
423 § 3.5 of Nixon et al. (2008a); (iii) the uncertainty in the line intensities of propane in the
424 spectral line lists, estimated at $\sim 10\%$.

425 The results show that the ν_{18} yields systematically higher values than the ν_{26} , com-
426 patible at the 2- σ error level but not at 1- σ . We suggest that two remaining systematic
427 effects are the sources of the difference: (i) any residual structure in the continuum at a
428 scale of less than 20 cm^{-1} for either spectral region that is not included in our slowly-
429 varying haze models, and (ii) any imperfections in the pseudo-linelist for the the ethane
430 ν_6 band at 1378 cm^{-1} . An actual linelist for the ν_6 and ν_8 bands would be very valuable
431 in eliminating this source of error.

432 We also note that the ν_{26} result is in very good agreement with the CIRS limb mea-
433 surement of Vinatier et al. (2007a) for 15°S, 3 mbar: $\sim 4 \pm 1.5 \times 10^{-7}$, also derived from
434 the ν_{26} band using a different (line-by-line) model and retrieval algorithm. Note that while
435 Vinatier et al. (2007a) did not scale the GEISA line intensities by the 0.42 factor used
436 by us, they partly compensated for the known problem with the ν_{26} band intensity by
437 omitting the vibrational part of the partition function when calculating the line strength.
438 This would tend to underestimate the line strengths, providing a similar correction factor
439 to ours, and the agreement between the results is not anomalous.

5 Summary and Conclusions

We have modeled a low-latitude limb spectral average of Titan, removing all gas emissions except propane. By examining the residual, we demonstrate that CIRS has detected at least six separate bands of C_3H_8 , including the well-known 748 cm^{-1} band (ν_{26}). We also show clearly the structure of the ν_7 band at 1158 cm^{-1} that underlies the ν_6 band of CH_3D ; the ν_{21} and ν_{20} bands at 922 and 1053 that were weakly detected by IRIS; and at least two others in the range $1300\text{--}1500\text{ cm}^{-1}$ (ν_{18} and ν_{24}) that are evident after the removal of methane emission. Detection of the weak ν_8 centered on 869 cm^{-1} that underlies the wing of the C_2H_6 ν_9 band is uncertain.

We have modeled the ν_{26} band using GEISA line data, and also the ν_{18} band using spectral line data from the work of Flaud et al. (2001). None of these determinations are problem-free: the ν_{26} band lacks spectroscopic data for the hot band lines at 749.5 cm^{-1} , whereas the ν_{18} band suffers from a lack of accurate continuum shape, and possible inaccuracies due to the use of the JPL pseudo-linelist for the ν_6 band of C_2H_6 , for which no formal lists are available. Despite these uncertainties, the values agree at a $2\text{-}\sigma$ error level. We suspect that systematic uncertainties (haze, ethane line list) are still of greater concern for FP4 than FP3, and therefore we recommend that the lower value $(4.2 \pm 0.5) \times 10^{-7}$, which agrees with previous analysis, is considered valid at the 2 mbar level for low latitudes probed by these retrievals.

Further work is required to accurately characterize the broad spectral features of Titan's mid-infrared continuum, as has been performed for the far-infrared (de Kok et al., 2007). Additional laboratory spectroscopy of alkanes is also required to support modeling of planetary spectra. It is vital that high-quality laboratory line lists are prepared for all bands of propane in the range $700\text{--}1300\text{ cm}^{-1}$, and also the ν_6 and ν_8 bands of ethane. The present lack of accurate spectral information is a serious obstacle, not only to accu-

465 rate measurement the abundance of propane on Titan and the giant planets, and deriving
466 underlying haze opacities, but also because our inability to model and remove propane's
467 prolific signature in many infrared spectral regions is a major hindrance to the search for
468 the signatures of new stratospheric trace species.

Acknowledgements

The acquisition of CIRS data is the result of the collective efforts of a large number of people, including the following who worked on various aspect of CIRS science planning, instrument commanding, uplink, calibration and databasing: S.B. Calcutt, R.C. Carlson, M.H. Elliott, E. Guandique, M. Kaelberer, E. Lellouch, A. Mamoutkine, P.J. Schinder, M.E. Segura, J.S. Tingley, and also many engineers and science planners at the Jet Propulsion Laboratory. We are indebted to J. Vander Auwera, for supplying us with the recent ethane ν_9 line data base in advance of its inclusion in the next GEISA release, and Steven Sharpe and colleagues at Pacific Northwest National Laboratory (PNNL) for the laboratory propane absorption spectra. We thank Geoff Toon and Armin Kleinboehl of JPL for the use of their C_2H_6 pseudo-linelist, which was generated using unpublished laboratory spectra recorded with Fourier transform spectrometers at the PNNL and the Kitt Peak National Observatory. We also thank W. Blass, G.L. Bjoraker, S. Daunt and T. Fouchet for e-mail exchanges regarding the GEISA propane data, and J.C. Brasunas for helpful discussions regarding aliasing and numerical filtering in the instrument. The US-based co-authors acknowledge the support of the NASA Cassini Project during the period in which this work was completed.

A Spectral range of CIRS FP4

The subject of the useable spectral range of CIRS FP4 is of considerable interest in this paper, due to the existence of many propane bands at the extremes of FP4 sensitivity. Further details of the CIRS spectral bandpass are available in an internal CIRS team report Brasunas (2004).

The nominal spectral range is 1100–1400 cm^{-1} , which significantly underestimates

492 the original bandpass: from 1020–1529 cm⁻¹, based on initial Nyquist sampling of the
 493 interferogram signal in the instrument. Frequencies from outside this range are aliased
 494 into the range, according to the formula:

$$495 \quad \tilde{\nu}_{\text{nominal}} + \tilde{\nu}_{\text{aliased}} = 2 \times \tilde{\nu}_{\text{bandpass}} \quad (\text{A.1})$$

496 A second-stage numerical filter is then applied that tapers the response towards the
 497 ends of the range, and leads to a definition of the ‘clean’ bandpass where the strength of
 498 the aliased signal has a relative response strength of less than 1%:

$$499 \quad \tilde{\nu}_{\text{clean}} = (2 \times \tilde{\nu}_{\text{bandpass}}) - \tilde{\nu}_{1\text{pc}} \quad (\text{A.2})$$

500 where $\tilde{\nu}_{1\text{pc}}$ is defined as the (aliased) frequency where the response of the numerical filter
 501 $R = F_{\text{FP4}}(\tilde{\nu})$ has dropped to 1% of the peak response: $\tilde{\nu}_{1\text{pc}} = F_{\text{FP4}}^{-1}(R_{\text{peak}} \times 0.01)$.
 502 By this definition, the clean bandpass of FP4 is 1131–1433 cm⁻¹, close to the canonical
 503 wavenumber range (1100–1400 cm⁻¹).

504 Between the Nyquist and ‘clean’ bandpass limits at the low wavenumber side (1020–
 505 1131 cm⁻¹), the aliased signal comes from the region 889–1020 cm⁻¹, where there is little
 506 emission except from the relatively weak lines of C₂H₄. In addition, roll-off of detector re-
 507 sponse at long wavelengths means that the ‘clean’ bandpass is somewhat underestimated.
 508 These effects mean that the range 1020–1131 cm⁻¹ is very useful, especially as the aliased
 509 spectral range 889–1020 cm⁻¹ is known from the FP3 spectrum and its importance can
 510 therefore be directly assessed.

511 The non-clean range from 1433–1529 is more problematic, because the detector reponse
 512 remains strong, and more critically because we have no knowledge of the signal in the
 513 aliasing range above 1529 cm⁻¹, except from predictions of emission bands of known
 514 gases (e.g. the weak ν_2 band of methane at 1534 cm⁻¹). Therefore, interpretation of this

515 spectral range must proceed with caution.

516 **B Modifications to propane spectral line lists**

517 In this work we used propane line data from two sources: (i) the GEISA atlas, for the ν_{26}
518 band at 748 cm^{-1} , and (ii) recent measurements by Flaud et al. (2001) for the bands in the
519 range $1300\text{--}1500\text{ cm}^{-1}$. During preliminary intercomparisons of the propane abundance
520 derived from the two spectral regions, we found large differences in the retrieved values
521 amounting to a factor ~ 2 (FP4 higher than FP3). We investigated possible causes of
522 this discrepancy, and discovered that the propane line strengths that are in the GEISA
523 2003 atlas are incorrectly scaled: this problem is expected to be fixed in the forthcoming
524 GEISA 2009 release, that should be available at the time of publication of this article.
525 We also suggest modifications to the Lorentzian Half-Width at Half Maximum (HWHM)
526 and temperature exponent of the spectral lines. A detailed discussion follows.

527 *B.1 Radiative Transfer Treatment of Spectral Lines*

528 For atmospheric radiative transfer applications we wish to compute the spectral depen-
529 dence of the absorption co-efficient k_ν for each molecular energy transition (i.e. spectral
530 line). Absorption due to all individual lines in a given spectral region is then included
531 in the overall opacity calculation, along with other sources (particles, collision-induced
532 opacity). Following Goody and Yung (1989), the spectral absorption due to an individual
533 line is:

$$534 \quad k_\nu = Sf(\nu - \nu_0) \tag{B.1}$$

535 where ν is frequency, ν_0 is the unperturbed frequency, f is a normalized function describing
 536 the line shape, and S is the line strength defined as:

$$537 \quad S = \int k_\nu d\nu \quad (\text{B.2})$$

538 The lineshape function may be given by the classical Doppler (thermal) or Lorentzian
 539 (pressure/collision) profiles, or more generally a convolution of both, known as the Voigt
 540 profile:

$$541 \quad f(\nu - \nu_0) = \int_{-\infty}^{+\infty} \frac{(\alpha_L/\pi)}{\left[\{(\nu - \nu_0) - (u\nu_0/c)\}^2 + \alpha_L^2 \right]} \left(\frac{m}{2\pi kT} \right)^{\frac{1}{2}} \exp\left(\frac{-mu^2}{2kT} \right) du \quad (\text{B.3})$$

542 In the above formula k , h and c are the usual constants of Boltzmann, Planck and speed
 543 of light; m is the molecular mass, T is temperature and α_L is the Lorentzian HWHM.

544 Therefore, in order to compute k_ν we must know the following: m and T , which are
 545 specified by the atmospheric problem; and α_L and S , which are parameters obtained from
 546 experimental measurement and tabulated in a database. Both of these parameters have
 547 a temperature dependence, and in addition α_L is a function of pressure also. First, the
 548 dependence of α_L on atmospheric conditions is specified by:

$$549 \quad \alpha_L(P, T) = \alpha_{L,0} \frac{P}{P_0} \left[\frac{T_0}{T} \right]^n \quad (\text{B.4})$$

550 where $(\alpha_{L,0}, P_0, T_0)$ is a laboratory (usually) room temperature measurement, and n is a
 551 free scaling parameter known as the Temperature Dependence of Width (TDW). Second,
 552 the line strength as a function of temperature is given by (e.g. Lacis and Oinas, 1991,
 553 p9033):

$$554 \quad S = S_0 \frac{V_0 R_0}{VR} \exp \left\{ \frac{hc}{k} E'' \left[\frac{1}{T_0} - \frac{1}{T} \right] \right\} \quad (\text{B.5})$$

555 where E'' is the energy of the lower state of the transition, and R and V are the rotational
 556 and vibrational *partition functions* (sums over microphysical state probabilities). The
 557 rotational partition function is $R(T) = T^x$ where $x = 1$ for linear molecules and $x = 3/2$
 558 for non-linear molecules, such as propane. The vibrational partition function is usually
 559 approximated by a quantum harmonic oscillator so that:

$$560 \quad V(T) = \prod_j (1 - \exp(-h\nu_j/kT))^{-g_j} \quad (\text{B.6})$$

561 where ν_j is the frequency of the j^{th} vibrational mode, for each of the 27 mode frequencies
 562 given in Table II, and g_j is the degeneracy of each mode, equal to 1 for this gas.

563 *B.2 GEISA Line Strengths for ν_{26}*

564 The spectroscopic line list provided in the current GEISA 2003 edition is unchanged
 565 since first added in 1991, and consists of ~ 9000 lines assigned by S. Daunt (unpublished)
 566 from room temperature spectra. S. Daunt (private communication) has told us that the
 567 integrated band intensity:

$$568 \quad S = \int_i S_i d\nu \quad (\text{B.7})$$

569 for ~ 3500 lines for the fundamental mode only (excluding hotbands - transitions from
 570 non-ground state energy levels) was scaled to match the band sum for the entire region
 571 as reported by Giver et al. (1984), which included hot bands. The value of S reported by
 572 Giver et al. (1984) is 4.33×10^{-19} cm molecule $^{-1}$, and we have separately estimated from
 573 the PNNL propane spectra a value of 4.27×10^{-19} cm molecule $^{-1}$, in good agreement.
 574 However, the integrated band intensity of the GEISA lines is slightly lower (3.76×10^{-19}
 575 cm molecule $^{-1}$). We have calculated $V(296K) = 2.71$, which is approximately the ratio
 576 of S for all transitions to ground state transitions only, and therefore, we estimate that

577 the S for the ν_{26} fundamental mode should be $(1/2.71) \times 4.27 \times 10^{-19} = 1.58 \times 10^{-19}$
578 cm molecule^{-1} . The strengths of individual lines in the atlas should therefore be scaled
579 by the ratio of the current GEISA S to the predicted: i.e. by $1.58/3.76 = 0.420$. We have
580 hence rescaled the GEISA lines for the ν_{26} band by this factor prior to computation of
581 the k -tables, which were used in our retrievals.

582 *B.3 Lorentz Broadening Parameters*

583 In the current GEISA 2003 edition, the Lorentz HWHM α_L is given as 0.08 cm^{-1}
584 for the ν_{26} band. However, the FWHM for the pressure broadening of C_3H_8 by N_2 has
585 been separately reported as 0.119 cm^{-1} by Nadler and Jennings (1989) (at 296 K) and
586 0.146 cm^{-1} by Hillman et al. (1992) (at 175 K). The latter authors also used these two
587 measurements at different temperatures to infer a value for the n exponent in Eq. B.4 of
588 0.50, which is lower than the 0.75 in GEISA at present. We have therefore adopted values
589 of $\alpha_{L,0} = 0.12 \text{ cm}^{-1}$ and $n = 0.50$ for all the bands of propane available to us, including
590 the FP4 bands.

591 **References**

- 592 Achterberg, R. K., Conrath, B. J., Gierasch, P. J., Flasar, F. M., Nixon, C. A., 2008.
593 Titan's middle-atmospheric temperatures and dynamics observed by the Cassini Com-
594 posite Infrared Spectrometer. *Icarus* 194, 263–277.
- 595 Bézard, B., Nixon, C., Kleiner, I., Jennings, D., 2007. Detection of $^{13}\text{CH}_3\text{D}$ on Titan.
596 *Icarus* 191, 397–400.
- 597 Brasunas, J. C., June 2004. Notes on CIRS spectra bandpasses. Tech. rep., NASA GSFC,
598 Greenbelt, MD 20771.
- 599 Coustenis, A., Achterberg, R., Conrath, B., Jennings, D., Marten, A., Gautier, D., Nixon,
600 C., Flasar, F., Teanby, N., Bézard, B., Samuelson, R., Carlson, R., Lellouch, E., Bjo-
601 raker, G., Romani, P., Taylor, F., Irwin, P., Fouchet, T., Hubert, A., Orton, G., Kunde,
602 V., Vinatier, S., Mondellini, J., Abbas, M., Courtin, R., 2007. The composition of Ti-
603 tan's stratosphere from Cassini/CIRS mid-infrared spectra. *Icarus* 189, 35–62.
- 604 Coustenis, A., Bézard, B., 1995. Titan's Atmosphere from Voyager Infrared Observations.
605 IV Latitude Variations of Temperature and Composition. *Icarus* 115, 126–140.
- 606 Coustenis, A., Bézard, B., Gautier, D., 1989a. Titan's Atmosphere from Voyager Infrared
607 Observations. I: The Gas Composition of Titan's Equatorial Region. *Icarus* 80, 54–76.
- 608 Coustenis, A., Bézard, B., Gautier, D., 1989b. Titan's Atmosphere from Voyager Infrared
609 Observations. II: The CH_3D Abundance and D/H Ratio from the 900–1200 cm^{-1} Re-
610 gion. *Icarus* 82, 67–80.
- 611 Coustenis, A., Jennings, D., Jolly, A., Bénilan, Y., Nixon, C., Vinatier, S., Gautier, D.,
612 Bjoraker, G., Romani, P., Carlson, R., Flasar, F., 2008. Detection of C_2HD and the
613 D/H ratio on Titan. *Icarus* 197, 539–548.
- 614 Coustenis, A., Salama, A., Schulz, B., Ott, S., Lellouch, E., Encrenaz, T., Gautier, D.,
615 Feuchtgruber, H., 2003. Titan's atmosphere from ISO mid-infrared spectroscopy. *Icarus*
616 161 (2), 383–403.

617 de Kok, R., Irwin, P., Teanby, N., Lellouch, E., Bézard, B., Vinatier, S., C.A., N., Fletcher,
618 L., Howett, C., Calcutt, S., Bowles, N., Flasar, F., Taylor, F., 2007. Oxygen compounds
619 in Titan's stratosphere as observed by Cassini CIRS. *Icarus* 186, 354–363.

620 Flasar, F., Kunde, V., Abbas, M., Achterberg, R., Ade, P., Barucci, A., Bézard, B., Bjo-
621 raker, G., Brasunas, J., Calcutt, S., Carlson, R., Césarsky, C., Conrath, B., Coradini, A.,
622 Courtin, R., Coustenis, A., Edberg, S., Edgington, S., Ferrari, C., Fouchet, T., Gautier,
623 D., Gierasch, P., Grossman, K., Irwin, P., Jennings, D., Lellouch, E., Mamoutkine, A.,
624 Marten, A., Meyer, J., Nixon, C., Orton, G., Owen, T., Pearl, J., Prangé, R., Raulin,
625 F., Read, P., Romani, P., Samuelson, R., Segura, M., Showalter, M., Simon-Miller, A.,
626 Smith, M., Spencer, J., Spilker, L., Taylor, F., 2004. Exploring the Saturn System in the
627 Thermal Infrared: The Composite Infrared Spectrometer. *Space Sci. Rev.* 115, 169–297.

628 Flasar, F. M., Achterberg, R. K., Feb. 2009. The structure and dynamics of Titan's middle
629 atmosphere. *Royal Society of London Philosophical Transactions Series A* 367, 649–664.

630 Flaud, J., Lafferty, W., Herman, M., 2001. First high resolution analysis of the absorption
631 spectrum of propane in the 6.7 μm to 7.5 μm spectral region. *J. Chem. Phys.* 114 (21),
632 9361–9366.

633 Fulchignoni, M., Ferri, F., Angrilli, F., Ball, A. J., Bar-Nun, A., Barucci, M. A., Bettanini,
634 C., Bianchini, G., Borucki, W., Colombatti, G., Coradini, M., Coustenis, A., Debei,
635 S., Falkner, P., Fanti, G., Flamini, E., Gaborit, V., Grard, R., Hamelin, M., Harri,
636 A. M., Hathi, B., Jernej, I., Leese, M. R., Lehto, A., Lion Stoppato, P. F., López-
637 Moreno, J. J., Mäkinen, T., McDonnell, J. A. M., McKay, C. P., Molina-Cuberos, G.,
638 Neubauer, F. M., Pirronello, V., Rodrigo, R., Saggin, B., Schwingenschuh, K., Seiff,
639 A., Simões, F., Svedhem, H., Tokano, T., Towner, M. C., Trautner, R., Withers, P.,
640 Zarnecki, J. C., 2005. In situ measurements of the physical characteristics of Titan's
641 environment. *Nature* 438, 785–791.

642 Gayles, J., King, W., 1965. The infrared spectrum of propane. *Spectrochem. Acta* 21,

643 543–557.

644 Giver, L., Varanasi, P., Valero, F., 1984. Propane absorption band intensities and band
645 model parameters from 680 to 1580 cm^{-1} at 296 and 200K. *J. Quant. Spectro. Rad.*
646 *Trans.* 31 (3), 203–213.

647 Goody, R., Yung, Y., 1989. *Atmospheric Radiation*, 2nd Edition. Oxford University Press,
648 Oxford, UK.

649 Hillman, J., Reuter, D., Jennings, D., Bjoraker, G., Blass, W., 1992. Extraterrestrial
650 spectroscopy: foreign-gas broadening of propane as it applies to the atmosphere of
651 Titan. *Spectrochem. Acta* 48A (9), 1249–1255.

652 Husson, N., Bonnet, B., Scott, N., Chedin, A., 1992. Management and study of spec-
653 troscopic information - the GEISA program. *J. Quant. Spectro. Rad. Trans.* 48 (5-6),
654 509–518.

655 Irwin, P., Teanby, N., de Kok, R., Fletcher, L., Howett, C., Tsang, C., Wilson, C., Calcutt,
656 S., Nixon, C., Parrish, P., 2008. The NEMESIS planetary atmosphere radiative transfer
657 and retrieval tool. *J. Quant. Spectro. Rad. Trans.* 109, 1136–1150.

658 Jacquinet-Husson, N., Scott, N. A., Chedin, A., Garceran, K., Armante, R., Chursin,
659 A. A., Barbe, A., Birk, M., Brown, L. R., Camy-Peyret, C., Claveau, C., Clerbaux,
660 C., Coheur, P. F., Dana, V., Daumont, L., Debacker-Barilly, M. R., Flaud, J. M.,
661 Goldman, A., Hamdouni, A., Hess, M., Jacquemart, D., Kopke, P., Mandin, J. Y.,
662 Massie, S., Mikhailenko, S., Nemtchinov, V., Nikitin, A., Newnham, D., Perrin, A.,
663 Perevalov, V. I., Regalia-Jarlot, L., Rublev, A., Schreier, F., Schult, I., Smith, K. M.,
664 Tashkun, S. A., Teffo, J. L., Toth, R. A., Tyuterev, V. G., Vander Auwera, J., Varanasi,
665 P., Wagner, G., Nov. 2005. The 2003 edition of the GEISA/IASI spectroscopic database.
666 *J. Quant. Spectro. Rad. Trans.* 95, 429–467.

667 Jennings, D. E., Flasar, F. M., Kunde, V. G., Samuelson, R. E., Pearl, J. C., Nixon, C. A.,
668 Carlson, R. C., Mamoutkine, A. A., Brasunas, J. C., Guandique, E., Achterberg, R. K.,

669 Bjoraker, G. L., Romani, P. N., Segura, M. E., Albright, S. A., Elliott, M. H., Tingley,
670 J. S., Calcutt, S., Coustenis, A., Courtin, R., Feb. 2009. Titan's Surface Brightness
671 Temperatures. *Astrophys. J. Lett.* 691, L103–L105.

672 Jennings, D. E., Nixon, C. A., Jolly, A., Bézard, B., Coustenis, A., Vinatier, S., Irwin,
673 P. G. J., Teanby, N. A., Romani, P. N., Achterberg, R. K., Flasar, F. M., 2008. Isotopic
674 Ratios in Titan's Atmosphere from Cassini CIRS Limb Sounding: HC₃N in the North.
675 *Astrophys. J. Lett.* 681, L109–L111.

676 Khare, B., Sagan, C., Arakawa, E., Suits, F., Callcott, T., Williams, M., 1984. Optical
677 constants of organic tholins produced in a simulated Titanian atmosphere: From soft
678 X-rays to microwave frequencies. *Icarus* 60, 127–137.

679 Kim, S., Caldwell, J., 1982. The abundance of CH₃D in the atmosphere of Titan, derived
680 from 8- to 14- μ m thermal emission. *Icarus* 52, 473–482.

681 Kunde, V. G., Ade, P. A., Barney, R. D., Bergman, D., Bonnal, J.-F., Borelli, R., Boyd,
682 D., Brasunas, J. C., Brown, G., Calcutt, S. B., Carroll, F., Courtin, R., Cretolle, J.,
683 Crooke, J. A., Davis, M. A., Edberg, S., Fettig, R., Flasar, M., Glenar, D. A., Graham,
684 S., Hagopian, J. G., Hakun, C. F., Hayes, P. A., Herath, L., Horn, L., Jennings, D. E.,
685 Karpati, G., Kellebenz, C., Lakew, B., Lindsay, J., Lohr, J., Lyons, J. J., Martineau,
686 R. J., Martino, A. J., Matsumura, M., McCloskey, J., Melak, T., Michel, G., Morell,
687 A., Mosier, C., Pack, L., Plants, M., Robinson, D., Rodriguez, L., Romani, P., Schaefer,
688 W. J., Schmidt, S., Trujillo, C., Vellacott, T., Wagner, K., Yun, D., Oct. 1996. Cassini
689 infrared Fourier spectroscopic investigation. In: Horn, L. (Ed.), *Proc. SPIE Vol. 2803*, p.
690 162-177, *Cassini/Huygens: A Mission to the Saturnian Systems*, Linda Horn; Ed. Vol.
691 2803 of Presented at the Society of Photo-Optical Instrumentation Engineers (SPIE)
692 Conference. pp. 162–177.

693 Lacis, A., Oinas, V., 1991. A description of the correlated- k distribution method for
694 modelling nongray gaseous absorption, thermal emission and multiple scattering in

695 vertically inhomogenous atmospheres. *J. Geophys. Res.* 96, 9027–9063.

696 Lebonnois, S., Rannou, P., Hourdin, F., Feb. 2009. The coupling of winds, aerosols and
697 chemistry in Titan’s atmosphere. *Royal Society of London Philosophical Transactions*
698 *Series A* 367, 665–682.

699 Maguire, W., Hanel, R., Jennings, D., Kunde, V., Samuelson, R., August 1981. C_3H_8 and
700 C_3H_4 in Titan’s atmosphere. *Nature* 292, 683–686.

701 Nadler, S., Jennings, D. E., Nov. 1989. Foreign-Gas Pressure-Broadening Parameters of
702 Propane Near 748 cm^{-1} . *Journal of Quantitative Spectroscopy and Radiative Transfer*
703 42, 399–.

704 Niemann, H. B., Atreya, S. K., Bauer, S. J., Carignan, G. R., Demick, J. E., Frost, R. L.,
705 Gautier, D., Haberman, J. A., Harpold, D. N., Hunten, D. M., Israel, G., Lunine, J. I.,
706 Kasprzak, W. T., Owen, T. C., Paulkovich, M., Raulin, F., Raaen, E., Way, S. H., 2005.
707 The abundances of constituents of Titan’s atmosphere from the GCMS instrument on
708 the Huygens probe. *Nature* 438, 779–784.

709 Nixon, C., Achterberg, R., Vinatier, S., Bézard, B., Coustenis, A., Irwin, P., Teanby, N.,
710 de Kok, R., Romani, P., Jennings, D., Bjoraker, G., Flasar, F., 2008a. The $^{12}C/^{13}C$
711 isotopic ratio in Titan hydrocarbons from Cassini/CIRS infrared spectra. *Icarus* 195,
712 778–791.

713 Nixon, C. A., 1998. Remote Sounding Of The Atmosphere of Titan. Ph.D. thesis, Uni-
714 versity of Oxford.

715 Nixon, C. A., Jennings, D. E., Bézard, B., Teanby, N. A., Achterberg, R. K., Coustenis,
716 A., Vinatier, S., Irwin, P. G. J., Romani, P. N., Hewagama, T., Flasar, F. M., 2008b.
717 Isotopic Ratios in Titan’s Atmosphere from Cassini CIRS Limb Sounding: CO_2 at Low
718 and Midlatitudes. *Astrophys. J. Lett.* 681, L101–L103.

719 Nixon, C. A., Teanby, N. A., Calcutt, S. B., Aslam, S., Jennings, D. E., Kunde, V. G.,
720 Flasar, F. M., Irwin, P. G. J., Taylor, F. W., Glenar, D. A., Smith, M. D., 2009. Infrared

721 limb sounding of Titan with the Cassini Composite InfraRed Spectrometer: effects of
722 the mid-IR detector spatial responses. *Appl. Optics* 48 (10), 1912–1925.

723 Rodgers, C., 2000. *Inverse Methods for Atmospheric Sounding. Series on Atmospheric,*
724 *Oceanic and Planetary Physics - Vol. 2.* World Scientific, Singapore.

725 Roe, H., Greathouse, T., Richter, M., Lacy, J., 2003. Propane on Titan. *Astrophys. J.*
726 597, L65–L68.

727 Rothman, L. S., Jacquemart, D., Barbe, A., Benner, D. C., Birk, M., Brown, L. R.,
728 Carleer, M. R., Chackerian, C., Chance, K., Coudert, L. H., Dana, V., Devi, V. M.,
729 Flaud, J. M., Gamache, R. R., Goldman, A., Hartmann, J. M., Jucks, K. W., Maki,
730 A. G., Mandin, J. Y., Massie, S. T., Orphal, J., Perrin, A., Rinsland, C. P., Smith,
731 M. A. H., Tennyson, J., Tolchenov, R. N., Toth, R. A., Vander Auwera, J., Varanasi,
732 P., Wagner, G., 2005. The HITRAN 2004 molecular spectroscopic database. *Journal of*
733 *Quantitative Spectroscopy and Radiative Transfer* 96, 139–204.

734 Sharpe, S., Johnson, T., , Sams, R., Chu, P., Rhoderick, G., Johnson, P., 2004. Gas-
735 Phase Databases for Quantitative Infrared Spectroscopy. *App. Spectroscopy* 58 (12),
736 1452–1461.

737 Shimanouchi, T., June 1972. *Tables of Molecular Vibrational Frequencies, Consolidated*
738 *Volume I.* Tech. Rep. 39, Nat. Stand. Ref. Data Serv., NBS.

739 Teanby, N., Irwin, P., de Kok, R., Nixon, C., Coustenis, A., Bézard, B., Calcutt, S., Bowles,
740 N., Flasar, F., Fletcher, L., Howett, C., Taylor, F., 2006. Latitudinal variations of HCN,
741 HC₃N and C₂N₂ in Titan’s stratosphere derived from Cassini CIRS data. *Icarus* 181,
742 243–255.

743 Teanby, N., Irwin, P., de Kok, R., Vinatier, S., Bézard, B., Nixon, C., Flasar, F., Calcutt,
744 S., Bowles, N., Fletcher, L., Howett, C., Taylor, F., 2007. Vertical profiles of HCN,
745 HC₃N and C₂H₂ in Titan’s atmosphere derived from Cassini/CIRS data. *Icarus* 186,
746 364–384.

747 Teanby, N. A., de Kok, R., Irwin, P. G. J., Osprey, S., Vinatier, S., Gierasch, P. J., Read,
748 P. L., Flasar, F. M., Conrath, B. J., Achterberg, R. K., Bézard, B., Nixon, C. A.,
749 Calcutt, S. B., Dec. 2008a. Titan’s winter polar vortex structure revealed by chemical
750 tracers. *Journal of Geophysical Research (Planets)* 113 (E12), 12003–+.

751 Teanby, N. A., Irwin, P., de Kok, R., Nixon, C., Coustenis, A., Royer, E., Calcutt, S.,
752 Bowles, N., Fletcher, L., Howett, C., Taylor, F., 2008b. Global and temporal variations
753 in hydrocarbons and nitriles in Titan’s stratosphere for northern winter observed by
754 Cassini/CIRS. *Icarus* 193, 595–611.

755 Teanby, N. A., Irwin, P. G. J., 2007. Quantifying the effect of finite field-of-view size
756 on radiative transfer calculations of Titan’s limb spectra measured by Cassini-CIRS.
757 *Astrophys. & Space Sci.* 310, 293–305.

758 Teanby, N. A., Irwin, P. G. J., de Kok, R., Nixon, C. A., Feb. 2009. Dynamical implications
759 of seasonal and spatial variations in Titan’s stratospheric composition. *Royal Society*
760 *of London Philosophical Transactions Series A* 367, 697–711.

761 Vander Auwera, J., Moazzen-Ahmadi, N., Flaud, J.-M., 2007. Towards an accurate
762 database for the 12 μm region of the ethane spectrum. *Astrophys. J.* 662, 750–757.

763 Vinatier, S., Bézard, B., Fouchet, T., Teanby, N. A., de Kok, R., Irwin, P. G. J., Con-
764 rath, B. J., Nixon, C. A., Romani, P. N., Flasar, F. M., Coustenis, A., 2007a. Vertical
765 abundance profiles of hydrocarbons in Titan’s atmosphere at 15°S and 80°N retrieved
766 from Cassini/CIRS spectra. *Icarus* 188, 120–138.

767 Vinatier, S., Bézard, B., Nixon, C., 2007b. The Titan $^{14}\text{N}/^{15}\text{N}$ and $^{12}\text{C}/^{13}\text{C}$ isotopic ratios
768 in HCN from Cassini/CIRS. *Icarus* 191, 712–721.

769 Vinatier, S., Bézard, B., Nixon, C. A., Mamoutkine, A., Guandique, E., Carlson, R. C.,
770 Jennings, D. E., Teanby, N. A., Bjoraker, G. L., Flasar, F. M., 2009. Analysis of
771 Cassini/CIRS limb spectra during the nominal mission. I. hydrocarbons, nitriles and
772 CO_2 vertical mixing ratio profiles. *Icarus* Submitted.

- 773 Wilson, E. H., Atreya, S. K., 2004. Current state of modeling the photochemistry of Ti-
774 tan's mutually dependent atmosphere and ionosphere. *Journal of Geophysical Research*
775 (Planets) 109 (E18), 6002–+.
- 776 Yung, Y., Allen, M., Pinto, J., 1984. Photochemistry of the atmosphere of Titan: Com-
777 parison between model and observations. *Astrophys. J. Supp.* 55, 465–506.

TABLE I
Titan Observational Data

Focal Plane	Spectral Range (cm ⁻¹)	Latitude Range	Mean Latitude	Altitude Range (km)	Mean Alt.(km)	No. of Spectra [†]	NESR [‡] (W cm ⁻² sr ⁻¹ /cm ⁻¹)
FP3	600–1100	30°S–30°N	9.5°N	100–150	130	568	3×10^{-9}
FP4	1100–1500	30°S–30°N	2.1°N	100–150	125	616	3×10^{-10}

[†] 2×10^5 space and 2×10^4 shutter spectra used in calibration.

[‡] NESR = Noise Equivalent Spectral Radiance ($1-\sigma$).

TABLE II
Propane IR Spectral Bands

Freq. (cm^{-1})	1972 No. [†]	1965 No. [‡]	Mode Type	Laboratory Spectra
————— CIRS FP1 —————				
216	14		Torsion	IR gas-phase inactive
268	27		Torsion	
369	9	9	CCC deform	
————— CIRS FP3 —————				
748	26	21	CH ₂ rock	Husson et al. (1992)
869	8	8	CC stretch	
922	21	16	CH ₃ rock	
940	13		CH ₃ rock	gas-phase inactive
————— CIRS FP3 & FP4 —————				
1053	20	15	CC stretch	
————— CIRS FP4 —————				
1158	7	7	CH ₃ rock	
1192	25	20	CH ₃ rock	
1278	12		CH ₂ twist	gas-phase inactive
1338	19	14	CH ₂ wag	Flaud et al. (2001)
1376	18	13	CH ₃ s-deform	Flaud et al. (2001)
1392	6	6	CH ₃ s-deform	
1451	11		CH ₃ d-deform	gas-phase inactive
1462	5	5	CH ₂ scissor	
1464	17	12	CH ₃ d-deform	
1472	24	19	CH ₃ d-deform	Flaud et al. (2001)
1476	4	4	CH ₃ d-deform	Flaud et al. (2001)
————— CIRS ENDS —————				
2887	16	3	CH ₃ s-str	
2887	3	11	CH ₂ s-str	
2962	2	2	CH ₃ s-str	
2967	10		CH ₃ d-str	gas-phase inactive
2968	23	18	CH ₂ a-str	
2968	15	10	CH ₃ d-str	
2973	22	17	CH ₃ d-str	
2977	1	1	CH ₃ d-str	

[†]Shimanouchi (1972) [‡]Gayles and King (1965)

TABLE III**Retrieved Propane VMR (ppm)**

Band	Grey Haze	Tholin
748 cm ⁻¹	$(4.2 \pm 0.5) \times 10^{-7}$	$(4.3 \pm 0.5) \times 10^{-7}$
1376 cm ⁻¹	$(5.7 \pm 0.8) \times 10^{-7}$	$(5.7 \pm 0.8) \times 10^{-7}$

Figure Captions

Fig. 1 Initial gas profiles for Titan spectral model. Upper plot: major isotopic species.
Lower plot: minor isotopic species.

Fig. 2 Plots of $W(z_i)$ spatial weighting function for limb spectral averages, resampled onto a 10 km grid relative to the mean tangent altitude, and normalized such that $\sum_i W(z_i) = 1.0$. Dashed line: FP3. Solid line: FP4. The effective weighting function of the final mean FP3 and FP4 spectra is different, due to two effects: (i) the different real detector spatial responses, and (ii) the slightly different distributions of center altitudes of the spectral sets comprising each average.

Fig. 3 A priori (dashed line) and retrieved temperature profile (solid line, with 1σ error bars) from Titan low-latitude (30°S – 30°N) spectral average from limb data (100–150 km tangent altitude). The grey shaded box shows the approximate region of real temperature information in the retrieval, as bounded by the min and max values of FWHM pressure levels of all temperature contribution functions assessed across the entire wavenumber range. At higher and lower levels the temperature profiles is smoothly joined to the *a priori*. A second weaker information region also exists above ~ 500 km due to methane hotband emissions.

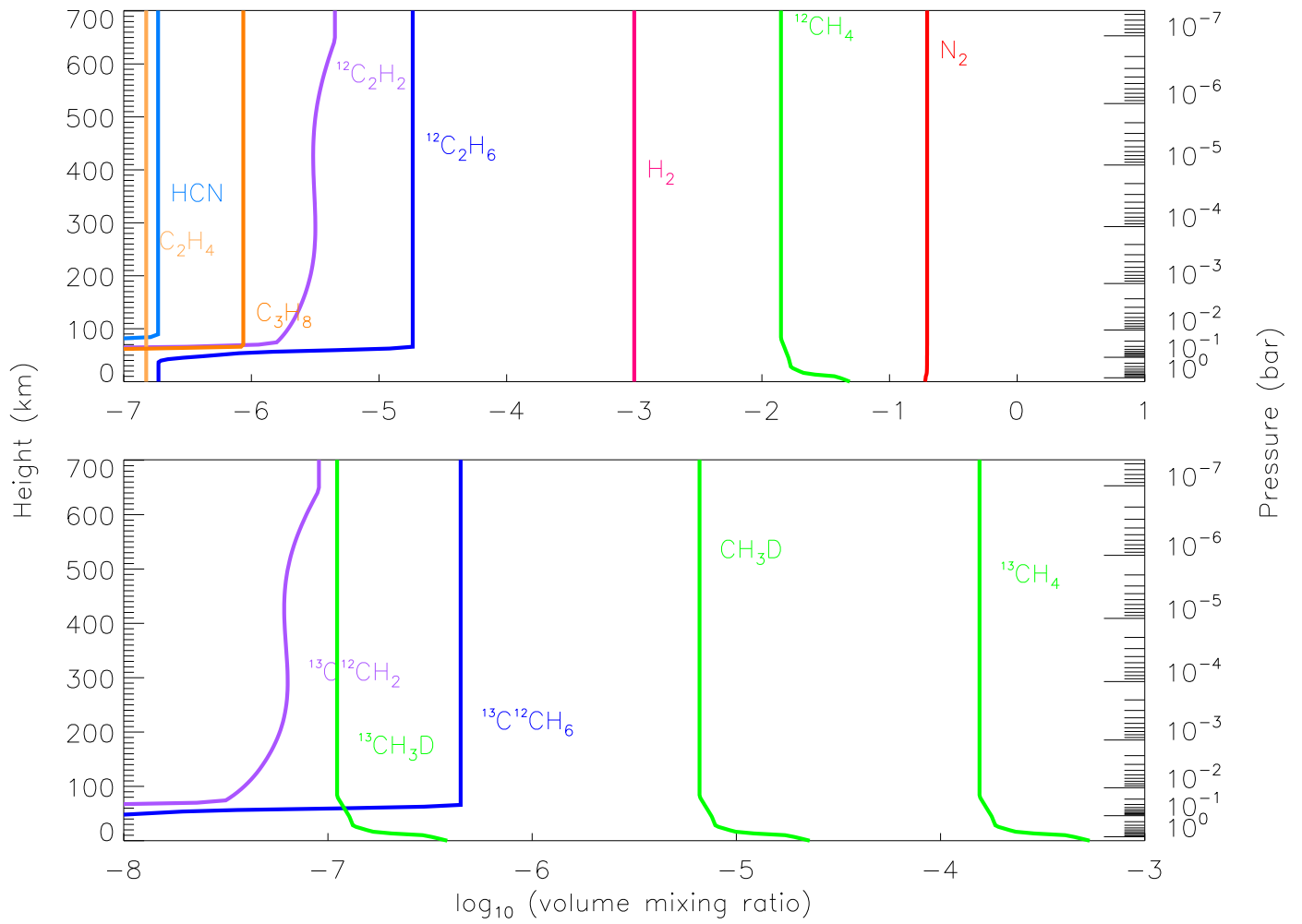
Fig. 4 Comparison of various contributions to the error on retrieved temperatures from fitting the methane ν_4 band. Dotted line: initial *a priori* error estimate. Dashed line: retrieval error due to spectral noise. Dot-dashed line: error due to methane abundance profile uncertainty. The combination of these two (spectral and methane profile errors) lead to the final vertical temperature error: solid line.

Fig. 5 Identification of propane spectral bands from CIRS Focal Plane 3 (600 – 1100 cm^{-1}). Left column: CIRS averaged limb spectra (9°N , 130 km), four selected data ranges (black line) and synthetic spectral fit (red) with all gases except C_3H_8 in model. Right column:

803 residual spectrum after model subtraction (red) compared to PNNL laboratory absorption
804 spectra (blue) and 1- σ NESR (grey). Propane bands are identified by text and dashed
805 lines. Note: incomplete removal of C_2H_6 ν_9 band emission is evident in the residual (d) at
806 840–850 cm^{-1} .

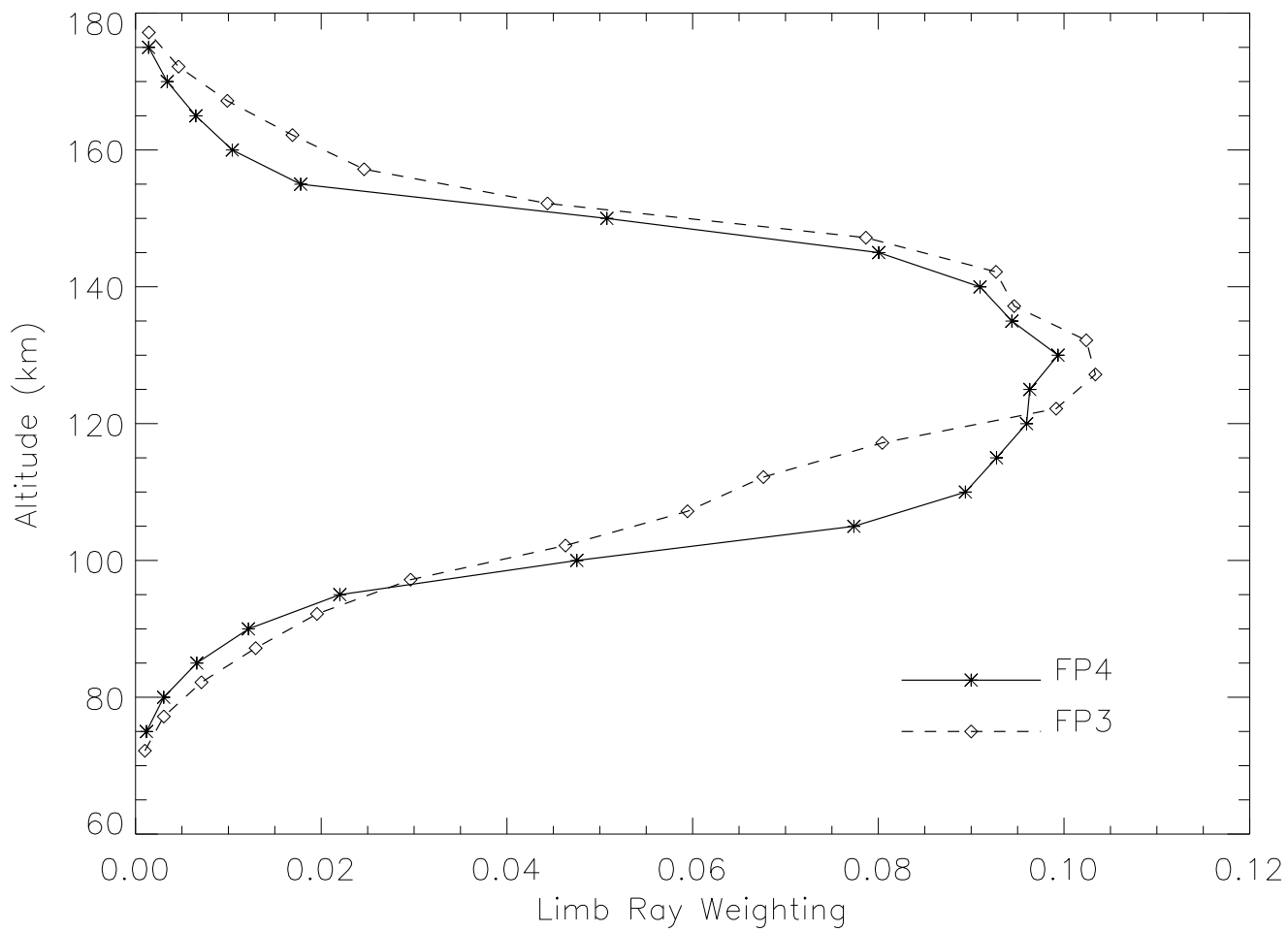
807 Fig. 6 Identification of propane spectral bands from CIRS Focal Plane 4 (1000–
808 1500 cm^{-1}). Left column: CIRS averaged limb spectra (2°N, 125 km), four selected data
809 ranges (black line) and synthetic spectral fit (red) with all gases except C_3H_8 in model.
810 Right column: residual spectrum after model subtraction (red) compared to PNNL labo-
811 ratory absorption spectra (blue) and 1- σ NESR (grey). Propane bands are identified by
812 text and dashed lines. Note: spectral baseline in the range 1440–1480 cm^{-1} (panel (h))
813 is not well modeled by grey haze, leading to over-estimation of the ethane abundance
814 (features marked with ‘*’) as the retrieval attempts to minimize the overall χ^2 of the fit.

815 Fig. 7 Residuals of fitting the two propane spectral regions. Red lines: residual of
816 forward calculation with no propane in model atmosphere, all other gases at previously
817 retrieved values. Blue line: residual after fitting with propane included, and grey haze
818 model. Green line: residual after fitting with propane included, and tholin particle haze
819 model. Grey bands are the 1- σ NESR. (a) ν_{26} band region, fitted by GEISA 2003 propane
820 line data modified as described in Appendix B. Note that the propane spectral data does
821 not include the hot band at 749.5 cm^{-1} , and also the significant difference to the ‘baseline’
822 level due to propane. (b) The ν_{18} band fitted with the recent spectral data of Flaud et al.
823 (2001).



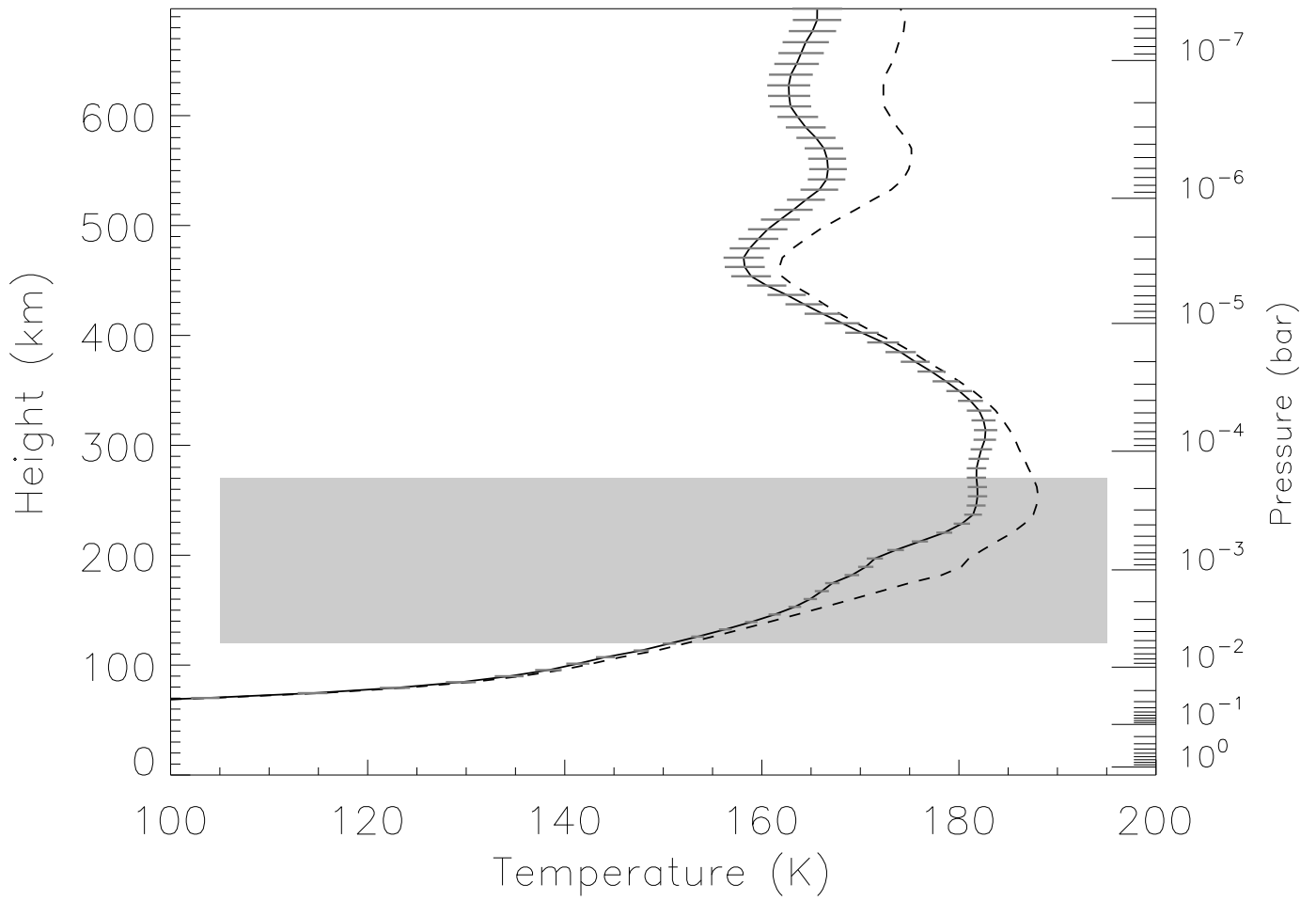
824

Nixon et al. **Figure 1**



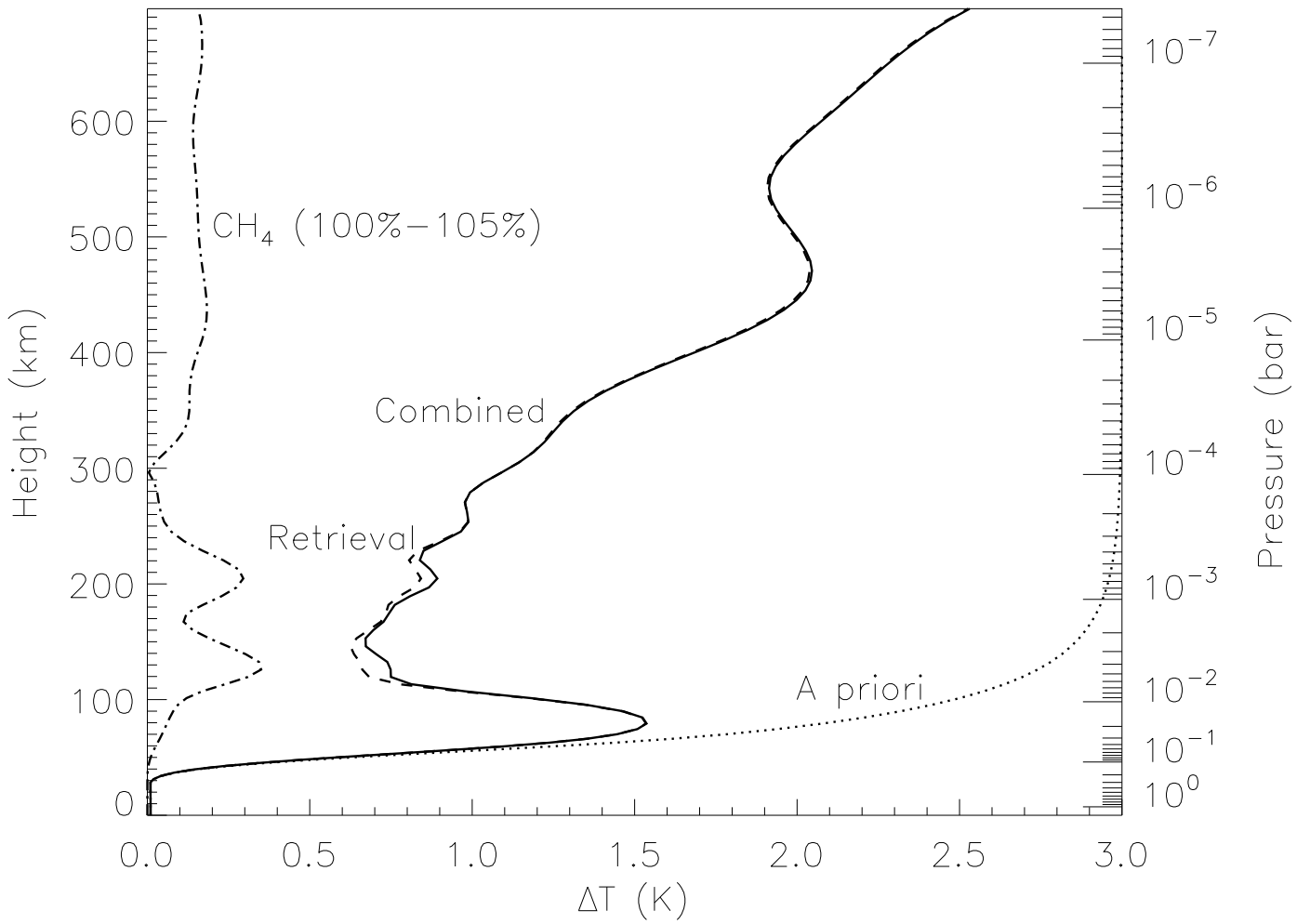
825

Nixon et al. **Figure 2**

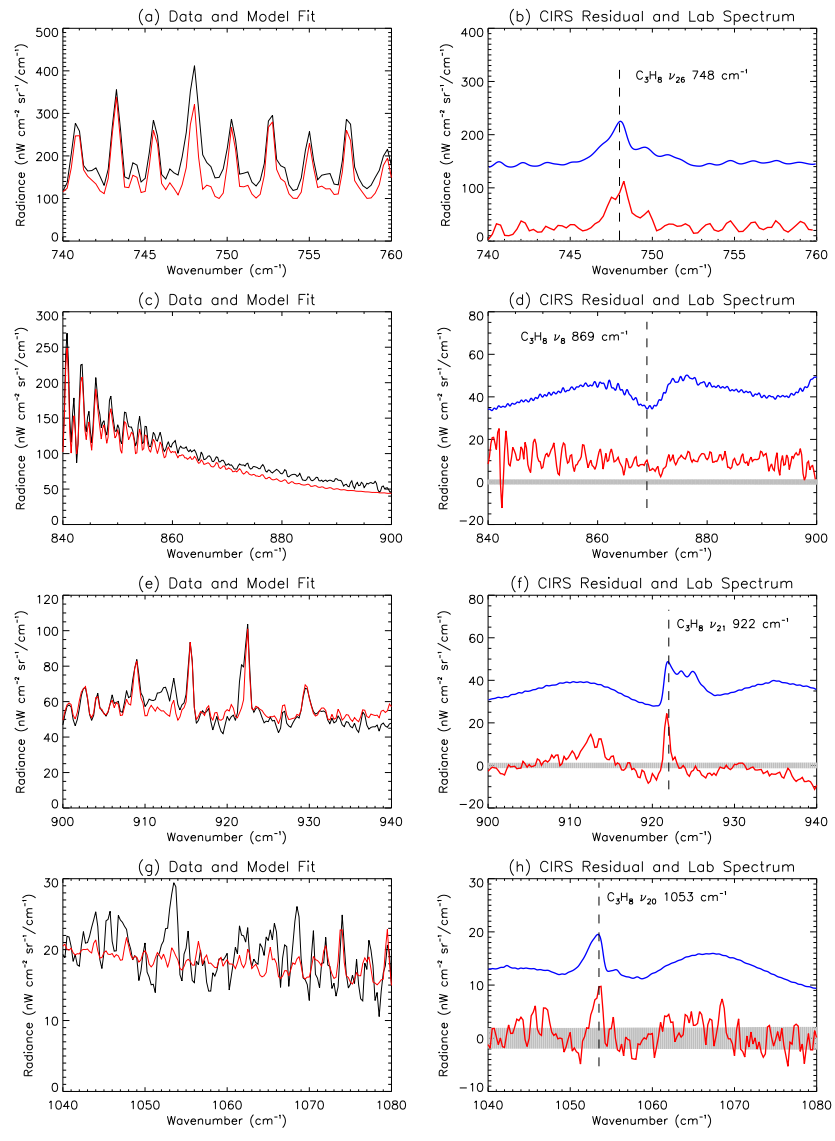


826

Nixon et al. **Figure 3**

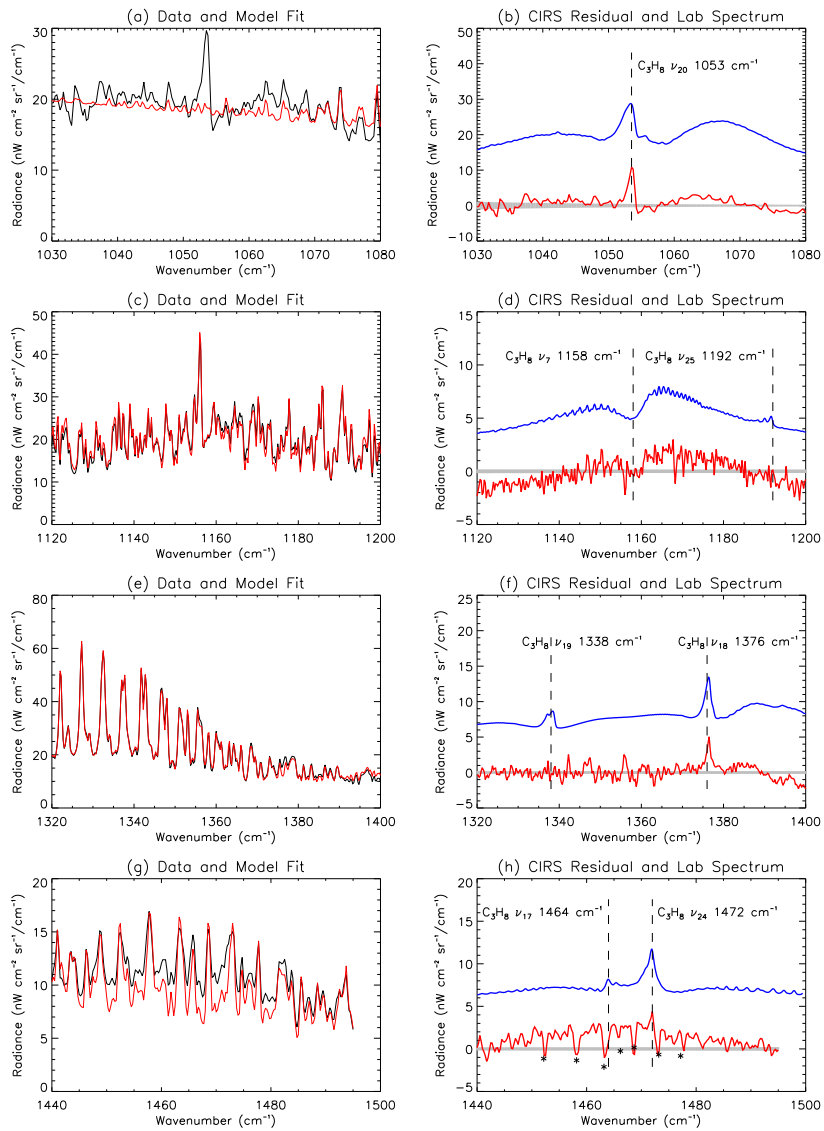


827 Nixon et al. **Figure 4**



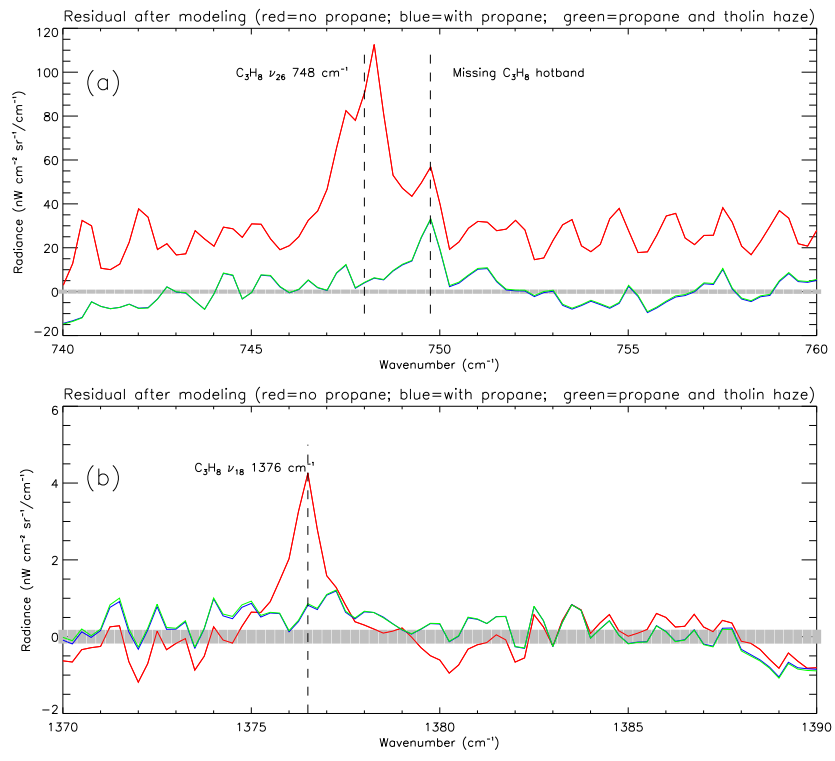
828

Nixon et al. **Figure 5**



829

Nixon et al. **Figure 6**



830

Nixon et al. **Figure 7**

This figure "nixon-c3h8-fig7.gif" is available in "gif" format from:

<http://arxiv.org/ps/0909.1794v1>